THE JOURNAL OF PHYSICAL CHEMISTRY Letters

Letter

pubs.acs.org/JPCL

Ab Initio Thermodynamics of Oxygen Vacancies and Zinc Interstitials in ZnO

Tor S. Bjørheim*,† and Eugene Kotomin‡,§

†Centre for Materials Science and Nanotechnology, Department of Chemistry, University of Oslo, Norway, FERMiO, Gaustadallén 21, 0349 Oslo, Norway

‡Max Planck Institute for Solid State Research, Heisenbergstrasse 1, 70569 Stuttgart, Germany

§Institute for Solid State Physics, University of Latvia, Kengaraga 8, 1063 Riga, Latvia

ABSTRACT: ZnO is an important wide band gap semiconductor with potential application in various optoelectronic devices. In the current contribution, we explore the thermodynamics of oxygen vacancies and zinc interstitials in ZnO from first-principles phonon calculations. Formation enthalpies are evaluated using hybrid DFT calculations, and phonons are addressed using the PBE and the PBE+U functionals. The phonon contribution to the entropy is most dominant for oxygen vacancies, and their Gibbs formation energy increases when including phonons. Finally, inclusion of phonons decreases the Gibbs formation energy difference of the two defects and is therefore important when predicting their equilibrium concentrations and the electrical activity of ZnO at finite temperatures.

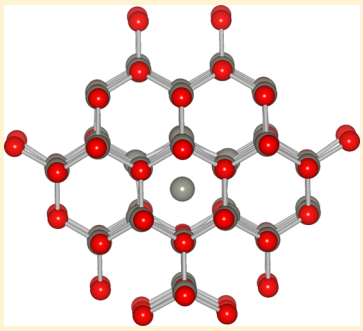

SECTION: Physical Processes in Nanomaterials and Nanostructures

ZnO is a wide band gap semiconductor that continues to attract considerable attention, mainly due to its optoelectronic properties, and finds potential application as transparent conducting electrodes and ultraviolet light-emitting diodes. As-grown ZnO usually displays a persistent n-type activity, which is attributed to various extrinsic defects, such as H, Al, and Si,[1−4] or intrinsic defects such as oxygen vacancies (v_O) and zinc interstitials (Zn_i).[5,6] Extensive efforts have been invested in both reducing the n-type activity and achieving effective p-type doping in order to realize various ZnO-based devices. A reoccurring challenge is, however, both the long-term stability and reproducibility of the p-type activity due to hole polaron trapping, self-compensation, defect complex formation, and high stability of donor defects such as H_i, v_O, and Zn_i.[5−9] Under reducing conditions, it is widely accepted that ZnO dissolves protons from H_2 gas through compensation by electrons[1,2,9]

$$\frac{1}{2}H_2(g) = H_i^{\bullet} + e' \tag{1}$$

Under H-free conditions, both v_O and Zn_i have been proposed as the dominating charged intrinsic donor defects.[5,10−13] However, their relative dominance at finite temperatures is difficult to predict a priori as they exhibit the same dependence on the oxygen activity

$$O_O^{\times} = v_O^{\bullet\bullet} + 2e' + \frac{1}{2}O_2(g) \tag{2}$$

$$Zn_{Zn}^{\times} + O_O^{\times} = Zn_i^{\bullet\bullet} + 2e' + \frac{1}{2}O_2(g) \tag{3}$$

First-principles studies have shown that Zn_i is a shallow donor while v_O displays a deep donor level.[5,6,14−16] Despite the deep donor behavior of v_O, both ionized Zn_i ($Zn_i^{\bullet\bullet}$) and v_O ($v_O^{\bullet\bullet}$) may act as charge-compensating defects in acceptor-doped ZnO. Further, the formation energy of $v_O^{\bullet\bullet}$ has been shown to be lower (0.5 eV) than that of $Zn_i^{\bullet\bullet}$,[6] leading to the assumption that the former defect is the preferred donor of the two.[5,6] The relative dominance of these two defects at finite temperatures is in addition affected by their formation entropy. The formation entropy is determined both by gas-phase and solid-state vibrational, that is, phonon, contributions. Gas-phase contributions are readily obtainable from, for instance, thermodynamic tables. Phonon contributions, on the other hand, require assessment of the vibrational properties of the defects. In this Letter, we address the phonon contribution to the free formation energy of $v_O^{\bullet\bullet}$ and $Zn_i^{\bullet\bullet}$ and explore their relative dominance as charge-compensating defects in ZnO at finite temperatures.

The first-principles calculations were performed with density functional theory as implemented in the VASP code,[17−20] using the GGA-PBE[21] and PBE+U[22] (with a Hubbard U-term of 5 eV for the Zn 3d orbitals) functionals for phonon calculations. The HSE functional[23,24] (intermixing 37% nonlocal Hartree−Fock exchange) was applied to calculate the electronic contributions to the defect formation energies. Further, we adopt the projector augmented wave (PAW)[25,26] method and a constant plane-wave cutoff of 700 eV (400 eV for HSE

Received: September 4, 2014
Accepted: October 20, 2014
Published: October 20, 2014

   dx.doi.org/10.1021/jz5018812 | J. Phys. Chem. Lett. 2014, 5, 4238−4242

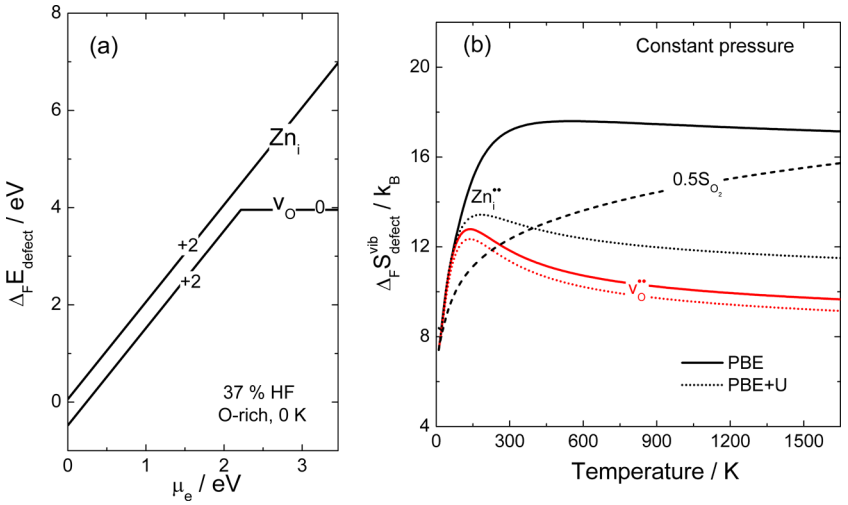

Figure 1. (a) Electronic formation energy of $Zn_i^{\bullet\bullet}$ and $v_O^{\bullet\bullet}$ from HSE as a function of the Fermi level and (b) formation entropy of $Zn_i^{\bullet\bullet}$ and $v_O^{\bullet\bullet}$ from PBE and PBE+U. The formation entropies are compared with half of the entropy of the free O_2 molecule, which represents the defect's formation entropy when neglecting phonon contributions.

calculations) to ensure interionic forces of sufficient accuracy. Structural optimizations were performed both by fixing the volume to that of the bulk supercell and by relaxing all volumes and shapes, in order to evaluate defect entropies under constant volume and zero/constant pressure conditions, respectively. Relaxation of the electronic system was performed to within an energy tolerance of 10^{-8} eV (10^{-6} eV for HSE), for self-consistency, while ionic optimizations were performed until all residual forces were smaller than 10^{-4} eV/Å (0.02 eV/Å for HSE). All defect calculations were performed with a $3 \times 3 \times 2$ expansion of the wurtzite unit cell with electronic integration performed over a $3 \times 3 \times 3$ **k**-mesh for the supercell ($2 \times 2 \times 2$ Γ-centered **k**-mesh for HSE). Although $Zn_i^{\bullet\bullet}$ can occupy both the tetrahedral and octahedral interstitial sites, we only address the octahedral configuration as this has been shown to be the energetically preferred configuration of the two.[5] The lattice parameters (a and c) calculated with the PBE, PBE+U, and HSE functionals were 3.287 and 5.305 Å, 3.235 and 5.205 Å, and 3.232 and 5.143 Å, respectively, in good agreement with the experimental values of 3.242 and 5.188 Å.[27]

Phonon calculations were performed within the harmonic approximation with finite displacements of 0.005 Å. Subsequent diagonalization and Fourier transform, and derivation of thermodynamics properties, was performed with the Phonopy code.[28] No LO/TO splitting was applied in this work. The phonon calculations allow us to determine the vibrational entropy and free energy of the perfect and defective systems

$$S^{\mathrm{vib}} = -k_{\mathrm{B}} \sum_{\mathbf{q},s} \ln\left[1 - \exp\left(-\frac{h\nu(\mathbf{q},s)}{k_{\mathrm{B}}T}\right)\right] + \frac{1}{T}\sum_{\mathbf{q},s}\left[\frac{h\nu(\mathbf{q},s)}{\exp\left(\frac{h\nu(\mathbf{q},s)}{k_{\mathrm{B}}T}\right) - 1}\right] \quad (4)$$

$$F^{\mathrm{vib}} = \sum_{\mathbf{q},s} h\nu(\mathbf{q},s) + k_{\mathrm{B}} \sum_{\mathbf{q},s} \ln\left[1 - \exp\left(-\frac{h\nu(\mathbf{q},s)}{k_{\mathrm{B}}T}\right)\right] \quad (5)$$

where $\nu(\mathbf{q},s)$ is the frequency of mode s at each **q**-point of the Brillouin zone (BZ). The phonon spectra are only evaluated at the Γ-point for the defective cells due to the large size of the supercell.

Defect formation energies (i.e., Gibbs/Helmholtz in the case of relaxed/constant volume) were evaluated according to

$$\Delta_{\mathrm{F}}F_{\mathrm{defect}} = (E^{\mathrm{tot}}_{\mathrm{defect}} - E^{\mathrm{tot}}_{\mathrm{bulk}}) + (F^{\mathrm{vib}}_{\mathrm{defect}} - F^{\mathrm{vib}}_{\mathrm{bulk}}) + \sum_i \Delta n_i \mu_i(T, p_i) + q(\mu_{\mathrm{e}} + \Delta\varepsilon) + p\Delta_{\mathrm{F}}V \quad (6)$$

where $E^{\mathrm{tot}}_{\mathrm{j}}$ is the total electronic energies of the defective and bulk supercells and $F^{\mathrm{vib}}_{\mathrm{j}}$ are the vibrational free energies according to eq 5. Further, Δn_i is the change in the number of atoms i with chemical potential μ_i, q is the effective charge of the defect, μ_{e} the Fermi level, and $\Delta\varepsilon$ aligns the core potentials of the perfect and defective supercells to remedy shifts in the band edges due to the jellium background charge. $\Delta_{\mathrm{F}}V$ is the formation volume of the defect, and the $p\Delta_{\mathrm{F}}V$ term was included for constant pressure conditions. By assuming thermal equilibrium at finite temperatures, the chemical potentials of O and Zn are related through

$$\mu_{\mathrm{ZnO}}(T,p) = \mu_{\mathrm{Zn}}(T,p) + \mu_{\mathrm{O}}(T,p) \quad (7)$$

The chemical potential of O is given by the chemical potential of O_2(g)

$$\mu_{\mathrm{O}}(T,p) = 0.5\left(\mu^{\circ}_{\mathrm{O_2}} + H_{\mathrm{O_2-zp}} + H_{\mathrm{O_2}}(T) - TS_{\mathrm{O_2}}(T) + k_{\mathrm{B}}T \ln\left(\frac{p_{\mathrm{O_2}}}{p^{\circ}}\right)\right) \quad (8)$$

where $H_{\mathrm{O_2-zp}}$, the zero-point energy (ZPE), is determined from the experimental vibrational modes of O_2, while $H_{\mathrm{O_2}}(T)$ and $S_{\mathrm{O_2}}(T)$ are obtained from thermodynamic tables.[29] Under the assumption of eq 7, the chemical potential of Zn is given by

dx.doi.org/10.1021/jz5018812 | J. Phys. Chem. Lett. 2014, 5, 4238−4242

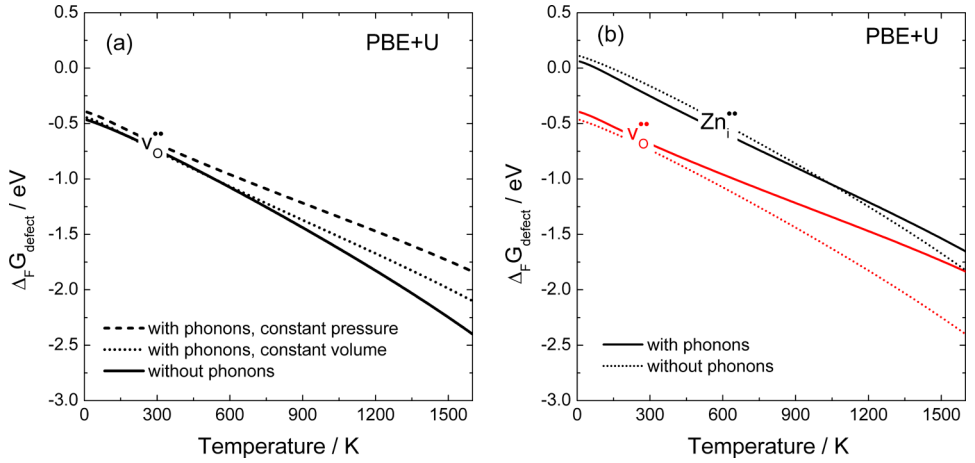

Figure 2. (a) The Helmholtz/Gibbs formation energy of $v_O^{\bullet\bullet}$ (with $\mu_e = \mu_{VBM}$) calculated with (constant volume or pressure) and without phonons. (b) The Gibbs formation energy of $v_O^{\bullet\bullet}$ and $Zn_i^{\bullet\bullet}$ (with $\mu_e = \mu_{VBM}$) with phonons (constant pressure) as a function of temperature under oxygen-rich conditions (p_{O_2} = 1 bar).

$$\mu_{Zn}(T, p) = \mu_{ZnO}(T, p) - \mu_O(T, p)$$
$$= \mu^{\circ}_{ZnO} + \mu_{ZnO}(T) - \mu_O(T, p) \quad (9)$$

where $\mu_{ZnO}(T)$ is obtained from the phonon calculations while $\mu^{\circ}_{O_2}$ and μ°_{ZnO} are the total, electronic energies from DFT. At finite temperatures, p_{O_2} was set to 1 bar, while at 0 K, this chemical potential limit corresponds to the "oxygen-rich" limit. The reader should again note that all electronic energies are evaluated by HSE calculations, while the entropies only are evaluated using PBE and PBE+U. Ideally, phonon contributions should also be evaluated using the HSE functional, but this was too computationally demanding for defective ZnO.

Figure 1a shows the formation energies (electronic contributions) from HSE under O-rich conditions. In line with the literature, we find that the Zn_i is a shallow donor, while v_O displays a deep (+2/0) transition level, 2.2 eV above the valence band maximum (VBM).[6,16] The electronic formation energy of $v_O^{\bullet\bullet}$ is 0.51 eV lower than that of $Zn_i^{\bullet\bullet}$. Figure 1b further shows the formation entropy of $v_O^{\bullet\bullet}$ and $Zn_i^{\bullet\bullet}$ calculated with PBE and PBE+U according to

$$\Delta_F S_{v_O^{\bullet\bullet}} = S^{vib}_{v_O^{\bullet\bullet}} - S^{vib}_{bulk} + 0.5 S_{O_2}(T) \quad (10)$$

$$\Delta_F S_{Zn_i^{\bullet\bullet}} = S^{vib}_{Zn_i^{\bullet\bullet}} - S^{vib}_{bulk} + 0.5 S_{O_2}(T) - S_{ZnO}(T) \quad (11)$$

The entropies are compared with $0.5 S_{O_2}(T)$, which represents the formation entropy of the defects without phonon contributions. While the calculated entropy of $v_O^{\bullet\bullet}$ is comparable with PBE and PBE+U, that of $Zn_i^{\bullet\bullet}$ is almost 50% higher with PBE than with PBE+U. Analyses revealed that this difference stems from unphysically large forces for certain displacements for $Zn_i^{\bullet\bullet}$ with PBE, affecting the low-frequency part of the phonon spectrum. These results thus indicate that the PBE+U method is more suitable for phonon analyses of ZnO rather than PBE. The phonon contributions evidently affect the formation entropy (and free energy) of both defects; their entropies at higher temperatures are lower than that of $0.5 S_{O_2}(T)$. At, for instance, 1000 K, the formation entropies of $v_O^{\bullet\bullet}$ and $Zn_i^{\bullet\bullet}$ are 9.6 and 11.9k_B, respectively, compared to 14.6k_B without phonons. Hence, the free energy of formation for both defects would be overestimated (too stable) when neglecting phonon contributions.

Figure 2a compares the formation energy of $v_O^{\bullet\bullet}$ calculated without phonons and with phonons under both constant volume (Helmholtz) and constant pressure (Gibbs) conditions. The formation energy of $v_O^{\bullet\bullet}$ is higher when including phonons, both under constant volume and constant pressure conditions. The formation energy is, further, slightly higher under constant pressure conditions than that under constant volume conditions, reflecting the negative phonon contribution to the formation entropy of $v_O^{\bullet\bullet}$ due to cell contraction ($\Delta_F V = -8.5$ Å^3/defect). Figure 2b compares the formation energy (Gibbs) of $v_O^{\bullet\bullet}$ and $Zn_i^{\bullet\bullet}$ calculated with and without phonons. The formation volume of $Zn_i^{\bullet\bullet}$ is also negative (−7.1 Å^3/defect), and the effect of volume relaxations on its formation entropy is therefore similar to that of $v_O^{\bullet\bullet}$. The effect of phonons on the free energy of formation of $Zn_i^{\bullet\bullet}$ is smaller than expected from the effect on the formation entropy, which stems from a negative vibrational enthalpy contribution to the formation energy.

The calculated phonon density of states of $v_O^{\bullet\bullet}$ and $Zn_i^{\bullet\bullet}$ (Figure 3) is very similar to that of the bulk spectrum in the low-frequency region. The major changes are the appearance of peaks at 300−350 and 590−610 cm^{-1} for $Zn_i^{\bullet\bullet}$ and 590 cm^{-1} for $v_O^{\bullet\bullet}$, similar to $v_O^{\times}$ in $SrTiO_3$.[30] These extra peaks could thus

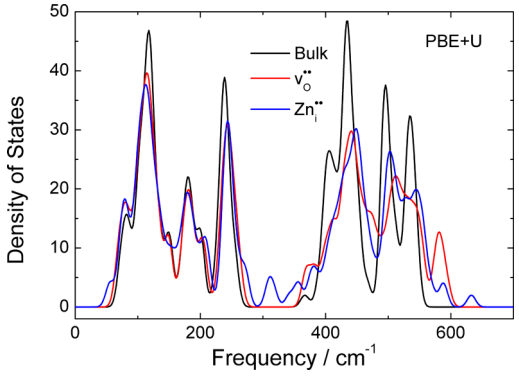

Figure 3. Phonon density of states of pure ZnO and cells with $v_O^{\bullet\bullet}$ and $Zn_i^{\bullet\bullet}$ defects, calculated at the Γ-point of the 3 × 3 × 2 supercell.

dx.doi.org/10.1021/jz5018812 | J. Phys. Chem. Lett. 2014, 5, 4238−4242

by used for defect identification by means of Raman spectroscopy.

To illustrate the effect of neglecting phonons on the prediction of defect concentrations in ZnO, we finally consider the case of 10^{-3} mole fraction (c_A) acceptor−doped ZnO in the hypothetical case where $v_O^{\bullet\bullet}$ and $Zn_i^{\bullet\bullet}$ act as the dominating defects, concentration-wise

$$2c_{v_O^{\bullet\bullet}} + 2c_{Zn_i^{\bullet\bullet}} = c_A \tag{12}$$

By taking the concentrations as

$$c_i = c_{s,x} \exp\left(-\frac{\Delta_F G_i}{k_B T}\right) \tag{13}$$

where $c_{s,x}$ is the concentration of regular sites (i.e., interstitial Zn sites, $c_{s,Zn}$, and O sites, $c_{s,O}$) while $\Delta_F G_i$ is given by eq 6. Combination of eqs 12 and 13 gives the following expression for the Fermi level (relative to a temperature-independent VBM)

$$\mu_e = -0.5k_B T \ln\left(\frac{c_A}{2}\right) + 0.5k_B T \ln\left[c_{s,Zn} \exp\left(-\frac{\Delta_F G_{Zn_i^{\bullet\bullet}}}{k_B T}\right) + c_{s,O} \exp\left(-\frac{\Delta_F G_{v_O^{\bullet\bullet}}}{k_B T}\right)\right] \tag{14}$$

Figure 4 compares the concentrations of $v_O^{\bullet\bullet}$ and $Zn_i^{\bullet\bullet}$ from eqs 12 and 13 and the corresponding equilibrium Fermi level (eq 14) as a function of temperature, with and without phonons. Although the formation energy of $Zn_i^{\bullet\bullet}$ itself is similar with and without phonons, the equilibrium concentration in this scenario is more than 1 order of magnitude higher when including phonons, which stems from the higher $\Delta_F G_{v_O^{\bullet\bullet}}$ and thus lower Fermi level, when including phonons in $\Delta_F G_{v_O^{\bullet\bullet}}$. The calculations predict Fermi levels in the p-type region of the band gap, both with and without phonons. The higher Fermi level when neglecting phonons, however, results in too low electron hole concentrations under equilibrium conditions in this scenario.

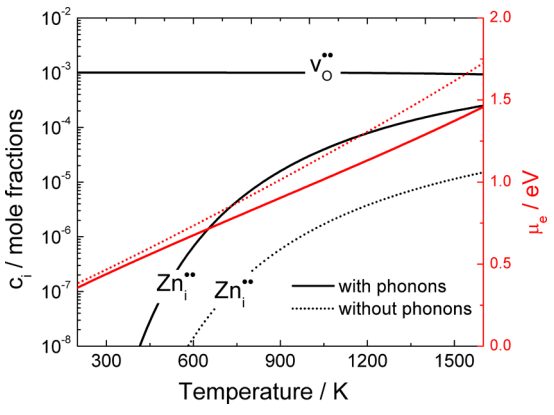

Figure 4. Concentrations of $v_O^{\bullet\bullet}$ and $Zn_i^{\bullet\bullet}$ in 10^{-3} mole fraction acceptor-doped ZnO in the hypothetical case where $v_O^{\bullet\bullet}$ and $Zn_i^{\bullet\bullet}$ are the dominating defects concentration-wise (eq 12). The red lines show the corresponding equilibrium Fermi level with respect to the VBM. The defect formation enthalpies are taken from HSE calculations in Figure 1a, while phonon contributions to the entropies are taken from PBE+U calculations.

The results of Figure 4 illustrate the importance of including phonon contributions in defect chemical analyses. Although such contributions can be small for certain defects, they could have large effects on other, dominating defects and thus be detrimental for accurate prediction of the equilibrium Fermi level and thus the concentration of all minority defects.

In conclusion, the PBE+U functional is more suitable for phonon calculations of ZnO. The calculated phonon contribution to the Gibbs formation energy is most pronounced for $v_O^{\bullet\bullet}$, thus reducing the formation energy difference of the two defects at high temperatures. Neglecting such contributions may therefore affect the predicted concentrations of both majority and minority defects and the Fermi level, and they are thus important when, for instance, judging whether specific dopants results in p-type ZnO.

AUTHOR INFORMATION

Notes

The authors declare no competing financial interest.

ACKNOWLEDGMENTS

The authors gratefully acknowledge the Research Council of Norway (project number 214252) and the Russian Science Foundation (project number 14-43-00052) for funding, and the Norwegian Metacenter for Computational Science for providing computational resources and excellent support under the project NN4604k. Finally, we thank the Max Planck Institute for Solid State Research in Stuttgart, Germany, for its hospitality during researcher exchange for the first author, and Prof. Reidar Haugsrud for helpful discussions and proof reading.

REFERENCES

(1) Thomas, D. G.; Lander, J. J. Hydrogen as a Donor in Zinc Oxide. *J. Chem. Phys.* **1956**, *25* (6), 1136−1142.
(2) Erdal, S.; Kjølseth, C.; Norby, T. Concentration and Mobility of Electrons in ZnO from Electrical Conductivity and Thermoelectric Power in H_2 + H_2O at High Temperatures. *J. Phys. Chem. C* **2010**, *114* (39), 16785−16792.
(3) Vines, L.; Monakhov, E. V.; Schifano, R.; Mtangi, W.; Auret, F. D.; Svensson, B. G. Lithium and Electrical Properties of ZnO. *J. Appl. Phys.* **2010**, *107* (10), 103707.
(4) Stehr, J. E.; Johansen, K. M.; Bjørheim, T. S.; Vines, L.; Svensson, B. G.; Chen, W. M.; Buyanova, I. A. Zinc-Vacancy−Donor Complex: A Crucial Compensating Acceptor in ZnO. *Phys. Rev. Appl.* **2014**, *2* (2), 021001.
(5) Janotti, A.; Van de Walle, C. G. Native Point Defects in ZnO. *Phys. Rev. B* **2007**, *76* (16), 165202.
(6) Oba, F.; Togo, A.; Tanaka, I.; Paier, J.; Kresse, G. Defect Energetics in ZnO: A Hybrid Hartree−Fock Density Functional Study. *Phys. Rev. B* **2008**, *77* (24), 245202.
(7) Zeng, Y. J.; Ye, Z. Z.; Xu, W. Z.; Li, D. Y.; Lu, J. G.; Zhu, L. P.; Zhao, B. H. Dopant Source Choice for Formation of p-Type ZnO:Li Acceptor. *Appl. Phys. Lett.* **2006**, *88* (6), 062107.
(8) Lyons, J. L.; Janotti, A.; Van de Walle, C. G. Why Nitrogen Cannot Lead to p-Type Conductivity in ZnO. *Appl. Phys. Lett.* **2009**, *95* (25), 252105.
(9) Bjørheim, T. S.; Erdal, S.; Johansen, K. M.; Knutsen, K. E.; Norby, T. H and Li Related Defects in ZnO and Their Effect on Electrical Properties. *J. Phys. Chem. C* **2012**, *116* (44), 23764−23772.
(10) Harrison, S. E. Conductivity and Hall Effect of ZnO at Low Temperatures. *Phys. Rev.* **1954**, *93* (1), 52−62.
(11) Hutson, A. R. Hall Effect Studies of Doped Zinc Oxide Single Crystals. *Phys. Rev.* **1957**, *108* (2), 222−230.

(12) Thomas, D. G. Interstitial Zinc in Zinc Oxide. *J. Phys. Chem. Solids* **1957**, *3* (3−4), 229−237.
(13) Hagemark, K. I. Defect Structure of Zn-Doped ZnO. *J. Solid State Chem.* **1976**, *16* (3−4), 293−299.
(14) Lany, S.; Zunger, A.; Many-Body, G. W. Calculation of the Oxygen Vacancy in ZnO. *Phys. Rev. B* **2010**, *81* (11), 113201.
(15) Gryaznov, D.; Blokhin, E.; Sorokine, A.; Kotomin, E. A.; Evarestov, R. A.; Bussmann-Holder, A.; Maier, J. A Comparative Ab Initio Thermodynamic Study of Oxygen Vacancies in ZnO and $SrTiO_3$: Emphasis on Phonon Contribution. *J. Phys. Chem. C* **2013**, *117* (27), 13776−13784.
(16) Clark, S. J.; Robertson, J.; Lany, S.; Zunger, A. Intrinsic Defects in ZnO Calculated by Screened Exchange and Hybrid Density Functionals. *Phys. Rev. B* **2010**, *81* (11), 115311.
(17) Kresse, G.; Hafner, J. *Ab Initio* Molecular Dynamics for Liquid Metals. *Phys. Rev. B* **1993**, *47* (1), 558−561.
(18) Kresse, G.; Hafner, J. *Ab Initio* Molecular Dynamics Simulation of the Liquid−Metal−Amorphous-Semiconductor Transition in Germanium. *Phys. Rev. B* **1994**, *49* (20), 14251−14269.
(19) Kresse, G.; Furthmüller, J. Efficiency of Ab-Initio Total-Energy Calculations for Metals and Semiconductors Using a Plane-Wave Basis Set. *Comput. Mater. Sci.* **1996**, *6* (1), 15−50.
(20) Kresse, G.; Furthmüller, J. Efficient Iterative Schemes for *Ab Initio* Total-Energy Calculations Using a Plane-Wave Basis Set. *Phys. Rev. B* **1996**, *54* (16), 11169−11186.
(21) Perdew, J. P.; Burke, K.; Ernzerhof, M. Generalized Gradient Approximation Made Simple. *Phys. Rev. Lett.* **1996**, *77* (18), 3865−3868.
(22) Dudarev, S. L.; Botton, G. A.; Savrasov, S. Y.; Humphreys, C. J.; Sutton, A. P. Electron-Energy-Loss Spectra and the Structural Stability of Nickel Oxide: An LSDA+U Study. *Phys. Rev. B* **1998**, *57* (3), 1505−1509.
(23) Heyd, J.; Scuseria, G. E.; Ernzerhof, M. Hybrid Functionals Based on a Screened Coulomb Potential. *J. Chem. Phys.* **2003**, *118* (18), 8207−8215.
(24) Krukau, A. V.; Vydrov, O. A.; Izmaylov, A. F.; Scuseria, G. E. Influence of the Exchange Screening Parameter on the Performance of Screened Hybrid Functionals. *J. Chem. Phys.* **2006**, *125* (22), 224106.
(25) Blöchl, P. E. Projector Augmented-Wave Method. *Phys. Rev. B* **1994**, *50* (24), 17953−17979.
(26) Kresse, G.; Joubert, D. From Ultrasoft Pseudopotentials to the Projector Augmented-Wave Method. *Phys. Rev. B* **1999**, *59* (3), 1758−1775.
(27) Albertsson, J.; Abrahams, S. C.; Kvick, A. Atomic Displacement, Anharmonic Thermal Vibration, Expansivity and Pyroelectric Coefficient Thermal Dependences in ZnO. *Acta Crystallogr., Sect. B* **1989**, *45* (1), 34−40.
(28) Togo, A.; Oba, F.; Tanaka, I. First-Principles Calculations of the Ferroelastic Transition between Rutile-Type and $CaCl_2$-Type SiO_2 at High Pressures. *Phys. Rev. B* **2008**, *78* (13), 134106.
(29) Chase, M. W., Jr. *NIST-JANAF Thermochemical Tables*, 4th ed.; The American Institute of Physics for the National Institute of Standards and Technology: New York, 1998.
(30) Evarestov, R.; Blokhin, E.; Gryaznov, D.; Kotomin, E. A.; Merkle, R.; Maier, J. Jahn−Teller Effect in the Phonon Properties of Defective $SrTiO_3$ From First Principles. *Phys. Rev. B* **2012**, *85* (17), 174303.